A Robust Hybrid CEEMDAN-IF-BiLSTM Framework for Accurate Short-Term Photovoltaic Power Forecasting

KHALED FERKOUS[1], BELGACEM BEKKAR[1], SARRA MENAKH[2], MAWLOUD GUERMOUI[3]
[1]Laboratory of Materials, Technology of Energy Systems and Environment (LMTESE)
Univercité de Ghardaia,
ALGERIA

[2]Laboratory of New and Renewable Energy in Aride Zones (LENREZA),
University Kasdi Merbah – Ouargla,
ALGERIA

[3]Renewable Energy Applied Research Unit (URAER),
Ghardaia,
ALGERIA

Abstract: — Predicting how much power solar panels will produce is a major hurdle for stable energy grids, largely because solar output is notoriously unpredictable, nonlinear, and constantly shifting. To tackle this, we've developed a hybrid deep learning framework designed for more accurate short-term forecasting. Our approach uses CEEMDAN to break down complex solar data into manageable components, paired with Iterative Filtering (IF) to pull out the most meaningful hidden patterns. These refined insights are then processed through a Bidirectional Long Short-Term Memory (BiLSTM) network. By combining these tools, our model captures the deep, time-sensitive relationships in solar generation that traditional methods often miss. Each component is then modeled using BiLSTM networks to capture bidirectional temporal dependencies, and the final forecast is obtained through signal reconstruction. The proposed model is evaluated using real-world PV datasets collected from Tindouf (Algeria), and its performance is compared with benchmark deep learning and decomposition-based approaches. Testing proves that this framework markedly boosts both the accuracy and reliability of solar power predictions. With an R^2 of $99.06\ \%$, an RMSE of 158.20 kW, and an nRMSE of 6.15%, the model consistently leads the way over standard LSTM models and other hybrid setups. These outcomes validate the idea that combining CEEMDAN decomposition, precise time-frequency feature extraction, and bidirectional deep learning creates a powerful, dependable solution for short-term forecasting. By blending these specific techniques, the system manages to capture the nuance of solar data more effectively than previous methods.

Key-Words: - Photovoltaic Power Forecasting; CEEMDAN; Instantaneous Frequency; BiLSTM; Hybrid Deep Learning; Time-Series Decomposition.

Received: May 13, 2025. Revised: September 5, 2025. Accepted: October 18, 2025. Published: December 31, 2025.

1 Introduction

The global shift toward sustainable, decentralized energy has sparked a decade of rapid expansion in photovoltaic (PV) power. This surge is fueled by a combination of aggressive environmental policies, significant cost drops in solar technology, and a worldwide push to cut carbon emissions. As a result, PV systems have moved from niche applications to a core component of modern power grids and international energy markets [1].

The inherent unpredictability and nonlinear nature of solar output create major hurdles for grid planning and daily operations. Because PV power is so sensitive to shifting cloud cover, flickering irradiance, and temperature swings, it introduces a high degree of uncertainty into generation profiles [2]. These sudden shifts make it difficult to balance the grid in real-time, manage power reserves, and ensure efficient dispatch; challenges that only intensify as energy systems become more dependent on renewables.

In this context, accurate short‑term forecasting (STF) of PV power plays a critical role in facilitating reliable grid integration and operational efficiency. Reliable STF enables better reserve allocation, improved scheduling of energy storage systems, and reduced dependence on expensive peaking plants, leading to operational cost savings and enhanced stability [3]. Even small improvements in forecasting accuracy can lead to measurable economic benefits and compliance with grid reliability standards [4].

Forecasting methods for PV generation can be generally divided into physical, statistical, and data-driven approaches. Physical forecasting models, frequently built on numerical weather predictions and radiative transfer equations, can achieve excellent accuracy but demand substantial environmental data and computational power [5]. Statistical techniques like autoregressive (AR) models and ARIMA are simple but frequently have difficulties with the nonlinear and non-stationary characteristics of PV time series [6]. To tackle model shortcomings, machine learning (ML) and deep learning (DL) methods have garnered significant focus in recent times.

These models are capable of recognizing intricate patterns in historical data and adjusting to the nonlinearity present in PV generation. Models like support vector regression and tree-based approaches have shown enhanced forecasting accuracy compared to conventional statistical methods [7]. Among DL architectures, Long Short-Term Memory (LSTM) networks excel at capturing temporal dependencies in time series, resulting in more precise predictions [8], [9].

Despite their promising performance, standalone deep learning models may encounter issues such as overfitting, sensitivity to noise, and limited capability to extract inherent signal features, especially in highly variable time‑series data [10]. To overcome these limitations, hybrid forecasting frameworks that integrate signal decomposition techniques with learning models have been increasingly proposed. Signal decomposition methods aim to separate complex time series into simpler, more regular components, enabling models to focus on salient temporal patterns while mitigating noise and irregular fluctuations [11], [12].

Common decomposition techniques explored in the literature include Empirical Mode Decomposition (EMD) [13], Ensemble Empirical Mode Decomposition (EEMD), Complete Ensemble Empirical Mode Decomposition with Adaptive Noise (CEEMDAN), and Wavelet Packet Decomposition (WPD) [14]. These methods enhance feature extraction and improve forecasting models' capacity to capture multi‑scale temporal dynamics [15]. Recent studies indicate that CEEMDAN‑based strategies can significantly improve short‑term PV forecasting by isolating intrinsic oscillatory modes, thus facilitating better predictive modelling [16].

An essential aspect of these hybrid approaches is the reconstruction of decomposed components. Proper reconstruction ensures that temporal coherence is maintained, leading to more robust and reliable forecasts [17]. While multiple stages of decomposition can improve feature extraction, excessive fragmentation of the signal may lead to increased computational complexity and reduced model efficiency, requiring careful design considerations [18].

Moreover, the integration of advanced feature extraction, such as iterative filtering (IF) analysis, has shown promise in capturing time‑frequency characteristics that standard decomposition techniques may not fully represent [19]. Combining these time‑frequency features with bidirectional deep learning models enables the capture of both past and future temporal dynamics, enhancing forecasting performance.

Motivated by these advances, this study proposes a hybrid forecasting framework based on CEEMDAN decomposition, iterative filtering feature extraction, and Bidirectional LSTM (BiLSTM) networks. The approach we are suggesting tries to make forecasts more reliable and accurate. The model works with real PV data from multiple PV plants, and its performance is compared with several baseline models, demonstrating significant improvements in forecast accuracy and reliability.

2 Methodology

2.1 Data Collection and Preprocessing

The empirical basis for this study consists of real-world measurements from a photovoltaic power plant located in Tindouf, Algeria. This dataset spans three consecutive annual cycles $(2021 - 2024)$, with power output recorded at 15-minute intervals. Such granular temporal resolution is vital for capturing the rapid, short-term fluctuations that characterize solar energy under actual operating conditions.

To ensure the model focuses on meaningful generation patterns, the preprocessing phase involved several key steps:

-**Data Filtering:** Nighttime observations with zero power output were removed to isolate periods of active energy production.

-**Feature Selection:** The forecasting task relies exclusively on historical power values; no external meteorological data or exogenous variables were used.

-**Normalization:** To maintain numerical stability and ensure consistent learning across different time periods, the data underwent **Z-score standardization** before being processed by the network.

2.2 Complete Ensemble Empirical Mode Decomposition with Adaptive Noise (CEEMDAN)

The original PV power time series was decomposed into a set of intrinsic mode functions (IMFs) using CEEMDAN. Each IMF captures a distinct oscillatory mode of the signal, enabling effective isolation of meaningful patterns and reduction of random noise. This decomposition enhances the ability of subsequent models to learn temporal dependencies and improves forecasting accuracy [20], [21].

2.3 Iterative Filtering (IF) Analysis

IF was employed as an alternative signal processing technique to analyze the PV power time series. Unlike traditional decomposition methods, IF iteratively extracts intrinsic mode components by applying adaptive filters to the signal, effectively separating oscillatory patterns from noise. The PV power signal was decomposed into a set of sub-signals that retain both temporal and spectral information, which are then used as inputs to the forecasting model. This approach enhances the model's ability to capture transient behaviors and subtle variations in PV output, particularly during high-fluctuation periods [22], [23].

2.4 Reconstruction Strategy

Following the prediction of each individual component obtained from VMD or WPD, a reconstruction strategy was applied to reassemble the final PV power forecast. This process involves summing the predicted sub-signals to approximate the original time series structure. The reconstruction not only ensures the temporal consistency of the forecast but also leverages the complementary information captured by each decomposed component. By integrating this step, the model mitigates cumulative prediction errors and achieves a more accurate and coherent power output forecast, especially when handling non-stationary and nonlinear behaviors in PV generation [24], [25]

2.5 Comparative Analysis

The proposed forecasting framework is anchored by a hybrid CEEMDAN-IF-BiLSTM architecture. This integrated approach leverages CEEMDAN to initially decompose the highly volatile PV signal, applies Iterative Filtering to further isolate and refine the extracted components, and utilizes BiLSTM networks to capture deep temporal dependencies. Finally, a reconstruction phase aggregates these component-level predictions into a cohesive, unified forecast, ensuring temporal consistency and a high-fidelity representation of the original power output.

To rigorously evaluate the effectiveness of this hybrid design, its performance is measured against several benchmark configurations. This ablation approach systematically isolates the contribution of each processing step:

-**Standard BiLSTM Model (Baseline):** This configuration directly forecasts the raw PV power time series without any signal decomposition or preprocessing. It establishes a baseline performance level, allowing for the precise quantification of gains achieved through the hybrid framework.

-**CEEMDAN-BiLSTM Model:** In this setup, the PV signal is decomposed into IMFs using CEEMDAN, and each IMF is modeled individually by a BiLSTM network. By omitting the secondary IF step, this model isolates and demonstrates the specific value of the primary decomposition phase.

-**IF-BiLSTM Model:** This configuration bypasses CEEMDAN entirely, applying Iterative Filtering directly to the raw data before BiLSTM processing. It is included to evaluate IF as a standalone signal-processing strategy.

By testing these distinct configurations against the fully integrated proposed model, this evaluation strategy provides a detailed, component-wise assessment. It clearly highlights how CEEMDAN decomposition, IF refinement, and BiLSTM temporal modeling synergize to deliver enhanced short-term PV power forecasting accuracy.

3 Experimental Setup

3.1 Data Collection and Site Description

The empirical data for this study originates from the Tindouf photovoltaic power plant in Algeria (Fig. 1). Designed for optimal energy yield, the facility operates with a total installed capacity of 23.92 MWp. This generation capacity is distributed across 93,792 individual PV modules, which are strategically configured into multiple identical blocks.

To capture the highly dynamic nature of solar generation under real-world operating conditions, historical power output was continuously logged over a comprehensive three-year period (2021 to 2024). These high-resolution measurements were recorded at $15-$minute intervals. Because the forecasting objective centers exclusively on active solar production, the dataset was preprocessed to systematically exclude all nighttime periods registering zero power output.

For rigorous model evaluation, the refined dataset was partitioned into distinct training and testing subsets. To preserve the chronological integrity of the time-series data, the initial portion of each year was allocated for model training, while the remaining periods were reserved to test predictive performance on unseen data. A detailed, seasonal breakdown of the descriptive statistics for the PV output (in kW) is provided in Table 1.

Table 1: Data exploration.

Data	Samples	Min	Max	Mean	STD
Winter	1893	7.92	5811.46	1904.44	960.75
Spring	2281	3.59	7260.37	2515.38	1629.38
Summer	2399	7.92	6033.15	2948.18	1837.88
Autumn	2004	7.92	6373.61	2827.11	1681.54
Average	1893	7.92	5811.46	1904.44	960.75

Source: created by the authors.

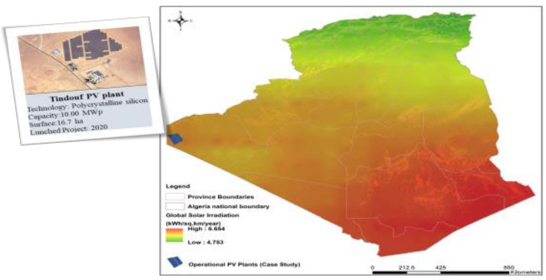

Fig. 1: Representation of the study zone in Tindouf.

3.2 Evaluation Metrics

To rigorously quantify the predictive performance of the proposed model, a comprehensive set of statistical evaluation metrics is employed. Relying on these standardized criteria ensures methodological rigor, allows for an objective comparison against conventional forecasting methods, and strongly supports the reproducibility of the findings [26].

3.2.1 Coefficient of Determination (R^2)

The coefficient of determination, commonly referred to as the goodness-of-fit, serves as a primary indicator of model accuracy. It defines the proportion of variance in the forecasted PV power that is predictable from the independent variables. An R^2 value approaching 1 indicates excellent explanatory power, meaning the model successfully captures the observed variability in the solar output [27].

$$R^2 = 1 - \frac{\left\|\mathbf{H}_{Obs} - \mathbf{H}_{pre}\right\|_2^2}{\left\|\mathbf{H}_{Obs} - \bar{H}_{Obs}\mathbf{1}\right\|_2^2} \tag{1}$$

where:

– $\mathbf{H}_{Obs} = \left[H_{1,Obs},\ H_{2,Obs}, \cdots, H_{N,Obs}\right]^T$ (observed values);
– $\mathbf{H}_{pre} = \left[H_{1,Obs},\ H_{2,Obs}, \cdots, H_{N,Obs}\right]^T$ (predicted values);
– $\bar{H}_{Obs} = \frac{1}{N}\sum_{n=1}^{N} H_{n,\mathrm{Obs}}$ (Mean of observed values);
– $\mathbf{1}$ denotes an $N \times 1$ vector of ones.

3.2.2 Bias

Bias is a critical statistical measure used to evaluate the average deviation of forecasted values from actual observations. In the context of grid management, it is vital to know whether a predictive model systematically overestimates or underestimates generation. A bias value approaching zero confirms the absence of systematic error, indicating a statistically unbiased model [28].

$$\text{Bias} = \frac{1}{\mathrm{N}}\mathbf{1}^{\mathrm{T}}(\mathbf{H}_{pre} - \mathbf{H}_{obs}) \tag{2}$$

3.2.3 Root Mean Square Error (RMSE)

RMSE is a fundamental metric for evaluating regression performance, measuring the average magnitude of the forecast errors. Because it squares the errors before averaging them, RMSE is particularly sensitive to large deviations or outliers. Lower RMSE values confirm a high degree of predictive accuracy [29].

$$\text{RMSE} = \sqrt{\frac{\left\|\mathbf{H}_{Obs} - \mathbf{H}_{pre}\right\|_2^2}{N}} \tag{3}$$

3.2.4 Normalized Root Mean Square Error (nRMSE)

To facilitate cross-dataset comparisons and evaluate the model across different measurement scales, the RMSE is normalized to create the nRMSE. Expressing the forecast error as a relative percentage

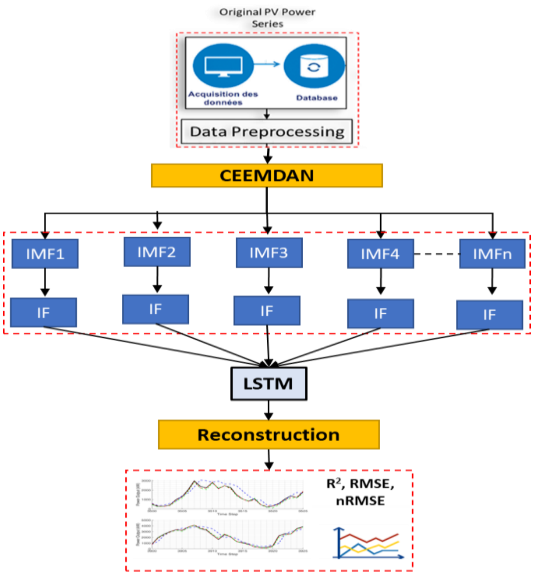

Fig. 2: Block diagram of the proposed hybrid forecasting framework.

Source: created by the authors.

provides a standardized view of model performance regardless of the plant's overall capacity [30].

$$nRMSE_{\%} = \frac{RMSE}{\overline{H}_{Obs}} \times 100\% \quad (4)$$

To interpret the nRMSE values, the following classification is adopted [26]:

- **Excellent**: nRMSE $<$ 5%
- **Good**: 5% $\leq$ nRMSE $<$ 10%
- **Fair**: 10% $\leq$ nRMSE $<$ 15%
- **Moderate**: 15% $\leq$ nRMSE $<$ 30%
- **Poor**: nRMSE $\geq$ 30%

The overall architecture and sequential workflow of the proposed forecasting framework, incorporating these evaluation stages, is comprehensively illustrated in Figure 2.

The proposed forecasting framework operates as a streamlined, multi-stage pipeline. Initially, the raw PV power time series undergoes preprocessing to remove zero-output nighttime periods and apply Z-score normalization. The refined signal is then decomposed using CEEMDAN, followed by IF to extract precise temporal-frequency features from each component. These isolated features are individually processed through BiLSTM networks, which effectively capture deep temporal dependencies across the data sequence. Finally, a reconstruction phase aggregates these component-level predictions into a unified, high-accuracy PV power forecast. Crucially, this modular design allows for a clear, component-wise evaluation of how each technique contributes to the overall predictive performance.

4 Results and discussions

To evaluate the accuracy and robustness of the proposed CEEMDAN-IF-BiLSTM model, a seasonal performance analysis was conducted. The main error metrics Bias, R^2, RMSE, and nRMSE were calculated for each season (Spring, Summer, Autumn, and Winter) as well as for the overall dataset. Table 2 (Appendix) presents the comparative results of the proposed method against several benchmark models, highlighting the impact of the adopted decomposition and signal processing strategy on forecasting performance.

As shown in Table 2 (Appendix), the proposed model consistently provides the most accurate predictions, achieving the highest R^2 values and the lowest RMSE and nRMSE across most seasons. While the baseline deep learning model shows larger errors and higher variability, decomposition-based approaches improve performance by reducing noise and isolating meaningful temporal patterns. The combination of CEEMDAN decomposition, instantaneous feature extraction, and BiLSTM learning leads to more stable and reliable forecasts, particularly under high-variability conditionsAs

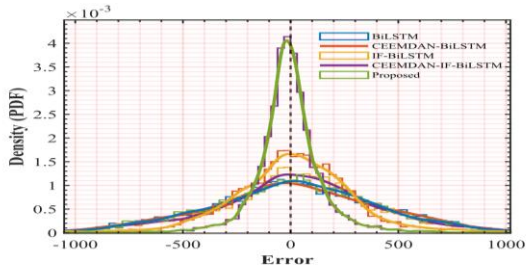

Fig. 3: Forecast Error PDFs for the Compared Models.

Source: created by the authors.

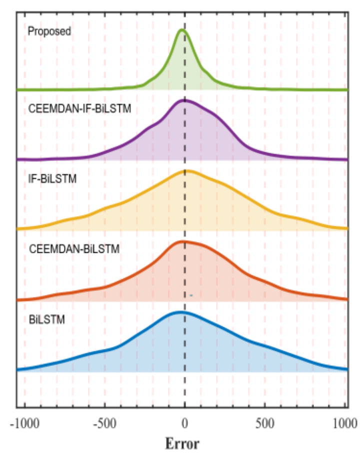

Fig. 4: Ridgeline Error Distributions Across Models.

Source: created by the authors.

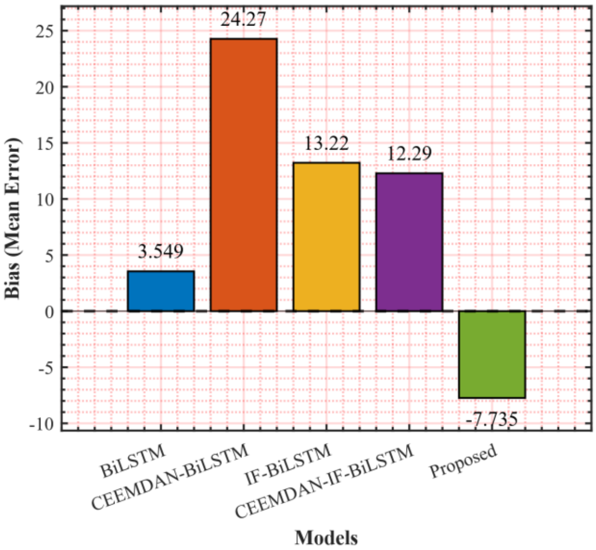

Fig. 5: Bias Comparison of Forecasting Models.

Source: created by the authors.

shown in Figure 3, the error PDFs reveal clear differences in how tightly predictions cluster around $Error = 0$. The Proposed model shows the sharpest peak near zero with lighter tails, indicating smaller errors and fewer extremes, while the other models have broader, heavier-tailed distributions. Overall, this tighter concentration confirms the Proposed model's improved accuracy and robustness.

As shown in Figure 4, the Proposed model has the narrowest, most centered error distribution around zero, indicating higher accuracy and fewer extreme errors, whereas the other models exhibit wider spreads that reflect greater variability and larger deviations.

Figure 5 shows noticeable differences in bias (mean error) across models. CEEMDAN -BiLSTM has the largest positive bias (strong overestimation), while IF-BiLSTM and CEEMDAN-IF-BiLSTM show moderate positive bias and BiLSTM a smaller one. In contrast, the Proposed model exhibits a negative bias, indicating slight underestimation and a more balanced behavior overall.

As shown in Figure 6, the error traces reveal clear differences in stability across the compared models: the baseline and hybrid variants exhibit wider fluctuations and more frequent high-amplitude spikes, indicating larger deviations from the target values over time. In contrast, the Proposed model maintains a visibly narrower error band with fewer extreme excursions, suggesting improved consistency and overall forecasting reliability.

Figure 7 shows the boxplots compare forecasting error distributions around the zero-error reference, where a narrower spread indicates better accuracy and stability. The Proposed model exhibits the tightest distribution and errors clustered closer to zero, while the other models show wider spreads and more outliers, implying greater variability and more frequent large deviations.

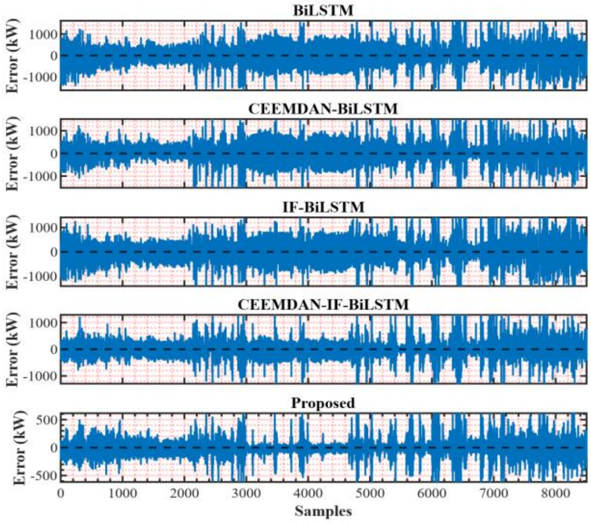

Fig. 6: Forecast Error Evolution Over Time for Different Models.

Source: created by the authors.

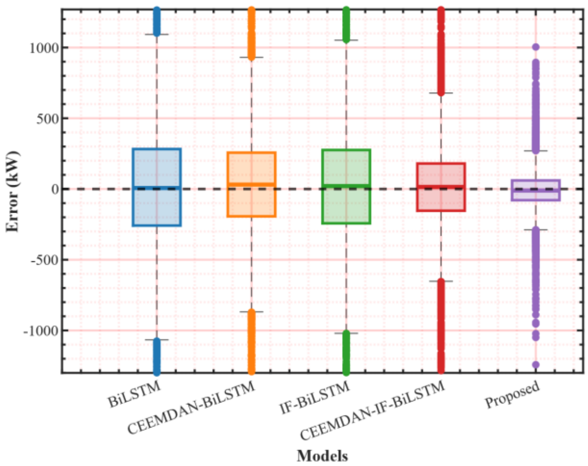

Fig. 7: Error Boxplot Comparison Across Models.

Source: created by the authors.

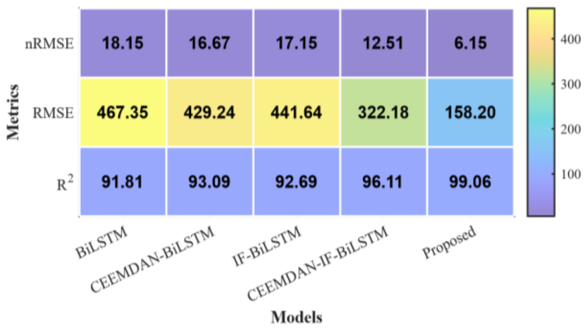

Fig. 8: Heatmap of Performance Metrics Across Forecasting Models.

Source: created by the authors.

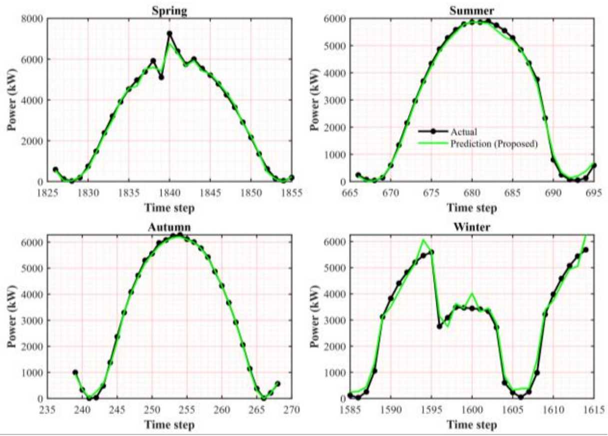

Fig. 9: Zoomed-In Forecast Comparison Over High-Variability Period.

Source: created by the authors.

The heatmap offers a concise visual comparison of the key performance metrics (R^2, RMSE, and nRMSE) across the evaluated models (Fig. 8).

As shown in Figure 8, BiLSTM exhibits the weakest overall accuracy, reflected by the highest error levels ($\text{RMSE} = 467.35\ kW, \text{nRMSE} = 18.15\%$) and the lowest coefficient of determination ($R^2 = 91.81$). In contrast, the Proposed model delivers the best performance, achieving the lowest $RMSE$ (158.20 kW) and nRMSE (6.15%) together with the highest R^2 (99.06%), indicating more reliable predictions and a substantial reduction in forecasting error compared with the other hybrid approaches.

To better evaluate the local prediction behavior of the models, Figure 9 presents a zoomed-in view of a selected segment from the test dataset. This excerpt, representing a high-variability period, highlights the differences in model accuracy during dynamic transitions. The LSTM model exhibits visible deviations, especially at rapid peaks and troughs. In contrast, decomposition-based models show improved alignment with the actual PV curve. Notably, the RVMD-LSTM model demonstrates the closest match to the ground truth, effectively capturing sharp changes and confirming its superior generalization ability under volatile conditions.

5 Conclusion

This study conducted a comprehensive evaluation of half-hour-ahead PV power forecasting using data from a newly considered PV station, comparing BiLSTM, CEEMDAN-BiLSTM, IF-BiLSTM, CEEMDAN-IF-BiLSTM, and the Proposed model. Overall, the Proposed approach achieved the most accurate and stable performance across the seasonal tests, attaining an average R^2 of 99.06, with $\text{RMSE} = 158.20\ \text{kW}$ and $\text{nRMSE} = 6.15\%$, while maintaining a small bias (-0.30). Relative to the baseline BiLSTM ($R^2 = 91.81\%, \text{RMSE} = 467.35\ \text{kW}, \text{nRMSE} = 18.15\%$), this corresponds to an error reduction of roughly 66%, and the gains remain consistent across different seasons.

Despite these strong results, the current setup has limitations. The models are trained only on historical PV power measurements, without incorporating exogenous drivers such as irradiance, temperature, wind speed, or cloud cover, which may reduce responsiveness to abrupt weather-induced changes. In addition, the validation is still limited to a single PV station, which may constrain generalization to other climates and operating conditions. Future work will therefore focus on integrating meteorological inputs, extending the framework to multi-step forecasting, and validating the method across multiple PV sites and climate zones to further improve robustness and practical deployment potential.

References:

[1] Y. Liu, J. Wang, L. Song, Y. Liu and L. Shen, "Enhanced Short-Term PV Power Forecasting via a Hybrid Modified CEEMDAN-Jellyfish Search Optimized BiLSTM Model," Energies, vol. 18, no. 13, p. 3581, 2025, doi: 10.3390/en18133581.

[2] Y. Li, S. Zhai, G. Yi, S. Pang and X. Luo, "Short-Term Photovoltaic Power Forecasting Based on ICEEMDAN-TCN-BiLSTM-MHA," Symmetry, vol. 17, p. 1599, 2025, doi: 10.3390/sym17101599.

[3] J. Zhang, Y. Hao, R. Fan and Z. Wang, "An Ultra-Short-Term PV Power Forecasting Method for Changeable Weather Based on Clustering and Signal Decomposition," Energies, vol. 16, no. 7, p. 3092, 2023, doi: 10.3390/en16073092.

[4] R. Zhang, Z. Xu, S. Liu, K. Fu and J. Zhang, "Prediction of Ultra-Short-Term Photovoltaic Power Using BiLSTM–Informer Based on Secondary Decomposition," Energies, vol. 18, p. 1485, 2025, doi: 10.3390/en18061485.

[5] D. Zhou, Y. Liu, X. Wang, F. Wang and Y. Jia, "Combined ultra-short-term photovoltaic power prediction based on CEEMDAN decomposition and RIME optimized AM-TCN-BiLSTM," Energy, vol. 318, p. 134847, 2025, doi: 10.1016/j.energy.2025.134847.

[6] J. Liang, L. Yin, Y. Xin, S. Li, Y. Zhao and T. Song, "Short-term photovoltaic power

prediction based on CEEMDAN-PE and BiLSTM neural network," Electric Power Systems Research, vol. 246, p. 111706, 2025, doi: 10.1016/j.epsr.2025.111706.

[7] M. Liu, X. Wang and Z. Zhong, "Ultra-Short-Term Photovoltaic Power Prediction Based on BiLSTM with Wavelet Decomposition and Dual Attention Mechanism," Electronics, vol. 14, p. 306, 2025, doi: 10.3390/electronics14020306.

[8] N. Zhang, Q. Ren, G. Liu, L. Guo and J. Li, "Short-term PV Output Power Forecasting Based on CEEMDAN-AE-GRU," Journal of Electrical Engineering & Technology, vol. 17, pp. 1183-1194, 2022, doi: 10.1007/s42835-021-00975-3.

[9] M. Ajith and M. Martínez-Ramón, "Deep learning algorithms for very short term solar irradiance forecasting: A survey," Renewable and Sustainable Energy Reviews, vol. 182, p. 113362, 2023, doi:10.1016/j.rser.2023.113362.

[10] A. Brihmat, H. Mahcene, D. Bechki, H. Bouguettaia, A. Khechekhouche and S. Boughali, "Energy Performance Improvement of a Solar Still System Using Date and Olive Kernels: Experimental Study," CLEAN – Soil, Air, Water, vol. 51, p. 2200384, 2023, doi: 10.1002/clen.202200384.

[11] N. Zhang, S. Wang, G. C. Liu and J. W. Zhang, "All-factor short-term photovoltaic output power forecast," IET Renewable Power Generation, vol. 16, pp. 148-158, 2022, doi: 10.1049/rpg2.12274.

[12] A. Yadav and S. Chandel, "Solar radiation prediction using Artificial Neural Network techniques: A review," Renewable and Sustainable Energy Reviews, vol. 33, pp. 772-781, 2014, doi: 10.1016/j.rser.2013.08.055.

[13] S. S. Chandel, A. Gupta, R. Chandel and S. Tajjour, "Review of deep learning techniques for power generation prediction of industrial solar photovoltaic plants," Solar Compass, vol. 8, p. 100061, 2023, doi: 10.1016/j.solcom.2023.100061.

[14] K. Ferkous, F. Chellali, A. Kouzou and B. Bekkar, "Wavelet-Gaussian Process Regression Model for Regression Daily Solar Radiation in Ghardaia, Algeria," Instrumentation Mesure Métrologie, vol. 20, pp. 113-119, 2021, doi: 10.18280/i2m.200208.

[15] C. Guo, X. Kang, J. Xiong and J. Wu, "A New Time Series Forecasting Model Based on Complete Ensemble Empirical Mode Decomposition with Adaptive Noise and Temporal Convolutional Network," Neural Processing Letters, vol. 55, pp. 4397-4417, 2023, doi: 10.1007/s11063-022-11046-7.

[16] R. Prasad, M. Ali, Y. Xiang and H. Khan, "A double decomposition-based modelling approach to forecast weekly solar radiation," Renewable Energy, vol. 152, pp. 9-22, 2020, doi: 10.1016/j.renene.2020.01.005.

[17] H. Wang, J. Sun and W. Wang, "Photovoltaic Power Forecasting Based on EEMD and a Variable-Weight Combination Forecasting Model," Sustainability, vol. 10, p. 2627, 2018, doi: 10.3390/su10082627.

[18] D. Niu, K. Wang, L. Sun, J. Wu and X. Xu, "Short-term photovoltaic power generation forecasting based on random forest feature selection and CEEMD: A case study," Applied Soft Computing, vol. 93, p. 106389, 2020, doi: 10.1016/j.asoc.2020.106389.

[19] C. Zhang, T. Peng and M. S. Nazir, "A novel integrated photovoltaic power forecasting model based on variational mode decomposition and CNN-BiGRU considering meteorological variables," Electric Power Systems Research, vol. 213, p. 108796, 2022, doi: 10.1016/j.epsr.2022.108796.

[20] T. Li, Z. Qian and T. He, "Short-Term Load Forecasting with Improved CEEMDAN and GWO-Based Multiple Kernel ELM," Complexity, vol. 2020, p. 1209547, 2020, doi: 10.1155/2020/1209547.

[21] H. Feng and C. Yu, "A novel hybrid model for short-term prediction of PV power based on KS-CEEMDAN-SE-LSTM," Renewable Energy Focus, vol. 47, p. 100497, 2023, doi: 10.1016/j.ref.2023.100497.

[22] U. K. Das, K. S. Tey, M. Seyedmahmoudian, S. Mekhilef, M. Y. I. Idris, W. Van Deventer, B. Horan and A. Stojcevski, "Forecasting of photovoltaic power generation and model optimization: A review," Renewable and Sustainable Energy Reviews, vol. 81, pp. 912-928, 2018, doi: 10.1016/j.rser.2017.08.017.

[23] S. M. Al-Selwi, M. F. Hassan, S. J. Abdulkadir, A. Muneer, E. H. Sumiea, A. Alqushaibi and M. G. Ragab, "RNN-LSTM: From applications to modeling techniques and beyond—Systematic review," Journal of King Saud University - Computer and Information Sciences, vol. 36, no. 5, p. 102068, 2024, doi: 10.1016/j.jksuci.2024.102068.

[24] H. Abbasimehr and R. Paki, "Improving time series forecasting using LSTM and attention models," Journal of Ambient Intelligence and Humanized Computing, vol. 13, no. 1, pp. 673-691, 2022, doi: 10.1007/s12652-020-02761-x.

[25] K. Ferkous, T. Boulmaiz, F. A. Ziari and B. Bekkar, "A hybrid approach based on complete ensemble empirical mode decomposition with adaptive noise for multi-step-ahead solar radiation forecasting," Clean Energy, vol. 6, pp. 705-715, 2022, doi: 10.1093/ce/zkac045.

[26] R. Bai, J. Li, J. Liu, Y. Shi, S. He and W. Wei, "Day-ahead photovoltaic power generation forecasting with the HWGC-WPD-LSTM hybrid model assisted by wavelet packet decomposition and improved similar day method," Engineering Science and Technology, an International Journal, vol. 61, p. 101889, 2025, doi: 10.1016/j.jestch.2024.101889.

[27] Y. Qu, J. Xu, Y. Sun and D. Liu, "A temporal distributed hybrid deep learning model for day-ahead distributed PV power forecasting," Applied Energy, vol. 304, p. 117704, 2021, doi: 10.1016/j.apenergy.2021.117704.

[28] N. L. M. Jailani, J. K. Dhanasegaran, G. Alkawsi, A. A. Alkahtani, C. C. Phing, Y. Baashar, L. F. Capretz, A. Q. Al-Shetwi and S. K. Tiong, "Investigating the Power of LSTM-Based Models in Solar Energy Forecasting," Processes, vol. 11, p. 1382, 2023, doi: 10.3390/pr11051382.

[29] K. Ferkous, M. Guermoui, S. Menakh, A. Bellaour and T. Boulmaiz, "A novel learning approach for short-term photovoltaic power forecasting - A review and case studies," Engineering Applications of Artificial Intelligence, vol. 133, p. 108502, 2024, doi: 10.1016/j.engappai.2024.108502.

[30] L. Cao, H. Yang, C. Zhou, S. Wang, Y. Shen and B. Yuan, "Photovoltaic Short-Term Output Power Forecast Model Based on Improved Complete Ensemble Empirical Mode Decomposition with Adaptive Noise–Kernel Principal Component Analysis–Long Short-Term Memory," Energies, vol. 17, p. 6365, 2024, doi: 10.3390/en17246365.

Contribution of Individual Authors to the Creation of a Scientific Article (Ghostwriting Policy)

The authors (Khaled Ferkous, Belgacem Bekkar, Sarra Menakh, and Mawloud Guermoui) equally contributed in the present research, at all stages from the formulation of the problem to the final findings and solution.

Sources of Funding for Research Presented in a Scientific Article or Scientific Article Itself

No funding was received for conducting this study.

Conflict of Interest

The authors have no conflicts of interest to declare that are relevant to the content of this article.

APPENDIX

Table 2: Seasonal Performance Metrics of Forecasting Models

Season	Metric	BiLSTM	CEEMDAN-BiLSTM	IF-BiLSTM	CEEMDAN-IF-BiLSTM	Peoposed
Average	R^2 (%)	91.81	93.09	92.69	96.11	99.06
	RMSE (kW)	467.35	429.24	441.64	322.18	158.20
	nRMSE (%)	18.15	16.67	17.15	12.51	6.15
	Bias (%)	0.14	0.94	0.51	0.48	-0.30
Spring	R^2 (%)	93.33	93.50	93.70	96.59	99.33
	RMSE (kW)	420.78	415.36	408.79	300.91	133.15
	nRMSE (%)	16.73	16.51	16.25	11.96	5.29
	Bias (%)	0.29	1.21	-0.27	0.46	-0.42
Summer	R^2 (%)	92.82	94.13	94.18	97.46	99.52
	RMSE (kW)	492.34	445.22	443.10	292.78	127.13
	nRMSE (%)	16.70	15.10	15.03	9.93	4.31
	Bias (%)	0.86	0.46	1.05	-0.44	-0.16
Autumn	R^2 (%)	90.17	91.61	91.19	94.16	98.40
	RMSE (kW)	527.17	487.02	499.08	406.10	212.39
	nRMSE (%)	18.65	17.23	17.65	14.36	7.51
	Bias (%)	-0.12	0.14	0.77	0.88	-0.02
Winter	R^2 (%)	81.04	86.49	81.59	91.55	97.42
	RMSE (kW)	418.18	353.01	412.14	279.25	154.28
	nRMSE (%)	21.96	18.54	21.64	14.66	8.10
	Bias (%)	-1.10	2.73	0.29	1.66	-0.81

Source: created by the author